merely scratch the surface of the rich phenomena awaiting investigation in the near future. We mention here, quite subjectively, a few of the problems that merit immediate exploration.

(1) Other surfaces, other mechanisms: For types of surfaces very different from those considered here, very different mechanisms of dissociation may become relevant. As mentioned in the review, Gadzuk and Holloway[17-19] proposed an electron jump mechanism which should apply to dissociation on metal surfaces and also perhaps to other substrates. Experimental demonstration of this should be very valuable. It seems very likely that still other new mechanisms of dissociation may exist, and a search for these mechanisms by theory and experiment should be of major interest.

(2) Polyatomic dissociation: Some of the most interesting questions for such systems are the branching ratios for different fragmentation processes, the internal energy distributions of the products, and the relevance of statistical models. No studies were reported on this topic.

(3) Vibrational excitation of molecules: While direct vibrational excitation was found unimportant for diatomic colliders, the situation may be very different for polyatomics, in particular those for which major rotational mode participation seems unlikely. Few reliable studies are available on vibrational energy transfer in surface collisions.

(4) Excitation of solid modes in the dissociation process: In addition to the shock-wave excitations described in this study and the familiar phonon excitations, other types of excitations may exist. For metals and semiconductors the electrons may also play a major role.

(5) Relation of collision-induced dissociation to "catalytic" dissociation: Although in the respective limiting cases the two processes are different, as argued at the outset of this review, intermediate behavior may well exist in suitable systems. Exploration of this point should be worthwhile.

It appears reasonable to expect, in view of the available experimental and theoretical technology, that rapid progress can be made on the many open problems in this field.

Acknowledgment. We are deeply indebted to our collaborators Drs. R. Elber and Z Bacic (Theory) and Dr. E. Kolodney (Experiment) whose role in much of the work described in this review was large. Work described here was supported by the U.S.–Israel Binational Science Foundation (by Grants No. 3209 and 3210 to the authors) and by the Foundation for Basic Research of the Israel Academy of Sciences. The Fritz Haber Research Center at The Hebrew University is supported by the Minerva Gesellschaft für die Forschung, mbH, München, BRD.

SPECTROSCOPY AND STRUCTURE

Multiple Scattered Wave Study of the Relativistic and Nonrelativistic Electronic Structure and Bonding for *cis*-Diamminedichloroplatinum(II)

Fernando Zuloaga*

Pontificia Universidad Católica de Chile, Facultad de Química, Casilla 6177, Santiago, Chile

and Ramiro Arratia-Pérez[†]

School of Engineering, University of Santa Clara, Santa Clara, California 95053
(Received: September 30, 1985)

A detailed analysis of the valence molecular orbitals of *cis*-$[Pt(NH_3)_2Cl_2]$ is presented. Ground-state results for the relativistic Dirac scattered wave (DSW) calculations and its nonrelativistic limit (DNR ($c = \infty$)) together with the nonrelativistic Schrödinger multiple scattered wave (MSW) results show the importance of relativistic effects in this molecule. The analysis yield interesting features; e.g., relativistic effects increase the relative splitting between levels containing significant 5d metal character. The Pauli decomposition for the orbitals showing large contributions from metal atoms suggests that spin contaminations are significant. Furthermore, the established MOs reveal that L → 5d(Pt) donation is low in comparison to L → 6p(Pt) donation so that metal p orbitals play a fundamental role in the bonding scheme for this molecule. Contour maps for the relativistic HOMO level show the existence of a Cl–Cl bonding region and suggest that an almost neutral ligand Cl_2 molecule exists in the complex, its free molecular electronegativity value is drastically reduced, and the Pt atom is responsible for this result.

I. Introduction

Over the past decade, the chemistry of the simple inorganic molecule *cis*-$[Pt(NH_3)_2Cl_2]$, cis-DDP, has undergone explosive growth, much of it due to the fortuitous discovery of its anticancer activity.[1] Its planar structure has been known for over a century, and its synthesis, physical properties, and reactions are continuously revised.[2] Despite these extensive efforts to understand its chemistry, little work has been done concerning its electronic structure and bonding properties. The review of Gray[3] in 1965 followed a SCF-X_α study[4] that was without success in both interpreting the spectral data and answering the question whether ordinary nonrelativistic quantum mechanical methods are appropriate for this molecule containing heavy atoms whose spin–

[†] Current address: Department of Chemistry, Simon Fraser University, Burnaby, B.C., Canada, V5A 1S6.

(1) Rosenberg, B.; van Camp, L.; Trosko, J. E.; Mansour, V. H. *Nature (London)* **1969**, *222*, 385.
(2) Lippard, S. J. *Science* **1982**, *218*, 1075.
(3) Gray, H. B. In *Transition Metal Chemistry*, Vol. 1, Carlin, R. L., Ed.; Arnold: London, 1965.
(4) Barber, M.; Clark, J. D.; Hinchliffe, A. *J. Mol. Struct.* **1979**, *57*, 169.

0022-3654/86/2090-4491$01.50/0

TABLE I: DSW Energy Levels and Valence Orbital Populations for *cis*-DDP in Terms of Atomic Spinors[a]

		Pt					2Cl			2N			$2H_{ax}$	$4H_{eq}$
level[b]	$-E$, eV	$s_{1/2}$	$p_{1/2}$	$p_{3/2}$	$d_{3/2}$	$d_{5/2}$	$s_{1/2}$	$p_{1/2}$	$p_{3/2}$	$s_{1/2}$	$p_{1/2}$	$p_{3/2}$	$s_{1/2}$	$s_{1/2}$
23e	2.2408	3.7	0.0	1.4	2.7	7.1	1.2	6.6	16.2	30.2	0.4	1.4	8.8	20.4
22e	2.3361	0.0	18.9	31.6	0.0	0.1	0.0	8.2	17.4	0.4	5.0	11.8	0.2	6.8
21e	2.5647	0.0	0.0	0.0	13.6	38.5	0.8	9.2	15.0	7.4	3.8	6.0	1.8	2.0
20e	5.9882	0.0	0.0	0.0	2.6	60.6	0.0	0.0	27.4	0.0	0.0	5.6	1.6	2.0
19e	6.4600	1.4	0.1	0.1	11.5	36.8	0.0	11.6	31.0	0.0	2.0	3.0	0.2	2.4
18e	6.5207	0.4	0.2	0.1	23.2	24.1	0.0	14.2	28.0	0.0	3.2	3.2	0.8	2.4
17e	6.8672	0.0	0.1	0.4	1.5	0.5	0.0	31.2	61.0	0.4	1.2	2.8	0.0	0.8
16e	7.4791	0.6	0.9	2.2	5.2	16.8	0.0	24.8	25.8	1.0	4.4	13.2	0.4	4.4
15e	7.5706	14.2	0.7	0.8	8.0	25.8	0.2	2.4	38.2	0.6	2.2	4.6	0.8	1.6
14e	7.8210	0.0	2.7	5.5	1.0	5.3	0.2	36.0	19.8	1.0	9.6	13.2	5.4	0.0
13e	7.9349	1.1	0.1	1.6	15.3	16.1	0.0	5.2	37.0	0.2	2.4	14.8	0.6	5.6
12e	8.2986	5.9	0.1	2.7	24.7	3.8	0.2	21.4	20.6	0.0	6.4	8.6	0.6	4.8
11e	8.4647	0.1	5.3	2.4	16.8	3.1	0.2	13.0	35.2	0.4	3.0	15.2	3.8	0.8
10e	9.0377	0.0	1.7	1.6	1.2	0.6	0.2	3.0	8.4	0.0	20.4	44.2	10.2	8.4
9e	9.5171	0.2	0.0	0.2	6.6	17.0	0.0	0.8	1.6	0.0	17.4	41.4	0.2	14.8
8e	9.7209	0.8	0.1	0.6	19.0	9.0	0.0	0.8	0.6	0.0	22.8	32.2	0.2	6.8
7e	10.0890	0.1	0.0	0.4	9.1	20.9	0.0	3.4	2.8	0.0	30.0	21.4	7.4	4.4
6e	10.7690	15.4	0.5	1.0	11.9	6.3	1.0	2.4	5.6	0.0	13.8	33.0	3.2	6.0
5e	10.9089	0.2	0.8	0.7	29.7	13.5	0.6	1.2	4.4	0.0	8.0	33.6	2.4	2.6
4e	19.5724	0.0	0.3	1.1	0.7	1.0	95.5	0.0	0.0	1.4	0.0	0.0	0.0	0.0
3e	19.6664	0.3	1.0	1.3	0.1	0.1	82.4	0.0	0.0	13.4	0.0	0.0	0.4	0.4
2e	20.0335	.0	0.6	1.0	2.2	3.0	1.2	0.0	0.0	84.2	0.0	0.0	2.6	5.2
1e	20.3173	5.2	0.3	0.5	0.9	1.2	14.0	0.0	0.0	71.4	0.0	0.0	2.0	4.4

[a] After partitioning the inner-sphere and outer-sphere charges. [b] The highest occupied level is 20e with d_{xz} (α) and [d_{z^2}, $d_{x^2-y^2}$] (β) and the spinor β is the largest contributor.

orbit parameters are large. Afterward, modified extended Hückel (EH) calculations with and without relativistic effects, followed by ligand corrections, were published.[5] Similar nonrelativistic extended Hückel methods were also used to support assignments of electronic transitions,[6] and the possible use of a semiempirical electrostatic potential approach to account for its biological properties was investigated recently.[7] However, its bonding properties have not been studied in great detail and a molecular orbital treatment that includes spin–orbit effects should be useful in the light of new thoughts about the bonding phenomena in complex molecules.

The current understanding of the bonding structure between metal and ligands is largely based on two charge-transfer mechanisms. First, the so-called ligand σ donation to metal d orbitals was considered to be the principal mechanism. Subsequently, theoretical and experimental analysis on simple octahedral compounds, especially hexacarbonyl complexes, indicated that significant back-donation from metal d to ligand π^* orbitals also exists.[8] Second, it has been found recently[9] that metal p orbitals also contribute to the mixing between different sets of σ and π orbitals, thereby allowing extra charge migration in the complex molecule.

The purpose of this work is to give a general description of the bonding for the *cis*-$[Pt(NH_3)_2Cl_2]$ compound and to make clear some issues[10] concerning its properties in terms of HOMO and LUMO characters. The analysis is based on MO calculations with both Slater[11] X_α self-consistent-field Dirac scattered wave method (DSW) developed by Yang and co-workers[12,13] and the traditional Schrödinger scattered wave (SW) technique of Johnson[14] for the ground and excited states.

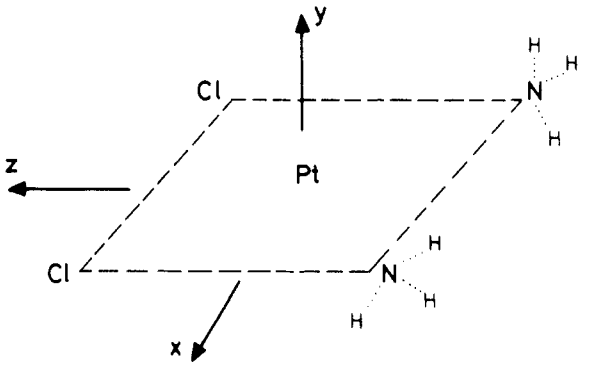

Figure 1. Coordinates system for *cis*-DDP in C_{2v} symmetry. Interatomic distances (in bohr) are 3.798 (Pt–N), 4.403 (Pt–Cl), 5.372 (N–N), 6.227 (Cl–Cl), and 5.496 (N–H). The sphere radii are 2.526 (Pt), 1.876 (Cl), 1.274 (N), and 0.673 (H).

In this paper section II outlines the computational details. Section III describes the ground-state results for the fully relativistic DSW calculations and its nonrelativistic limit DNR ($c = \infty$) together with the nonrelativistic Schrödinger SWX_α, including transition-state analysis. Finally, the bonding scheme for *cis*-DDP is discussed in section IV.

II. Computational Details

Figure 1 shows the molecular Cartesian axis for the *cis*-$[Pt(NH_3)_2Cl_2]$ molecule together with the sphere radii chosen for each atom to satisfy the experimental atomic distances[15] in the touching sphere method. The atomic X_α values were those of Schwarz[16] and the basis set in C_{2v} symmetry for the DWS and the nonrelativistic Schrödinger method were minimal with $l \leq 4$, $l \leq 2$, and $l \leq 1$ for the outer, metal, and ligand atoms, except for hydrogen for which $l = 0$ was used. Orbital energies were calculated with a convergence of 8.5×10^{-5} Ry for the fully relativistic calculation and its $c = \infty$ limit. Schrödinger results[17] were converged to 1-mRy potential energy. For both methods

(5) Carsey, T. P.; Boudreaux, F. A. *Theor. Chim. Acta* **1980**, *56*, 211.
(6) Patterson, H. H.; Tewksburg, J. C.; Martin, M.; Krogh-Jespersen, M. B.; Lo Menzo, J. A.; Hooper, H. O.; Viswanath, A. *Inorg. Chem.* **1981**, *20*, 2297.
(7) Abdul-Abad, P. G.; Webb, G. A. *Int. J. Quantum Chem.* **1982**, *21*, 1105.
(8) (a) Hubbard, J. L.; Lichtenberger, D. L. *J. Am. Chem. Soc.* **1982**, *104*, 2132. (b) Rees, B.; Mitschler, A. *J. Am. Chem. Soc.* **1976**, *98*, 7918.
(9) Arratia-Pérez, R.; Yang, C. *J. Chem. Phys.* **1985**, *83*, 4005.
(10) Cleare, M. J.; Hydes, P. C. In *Metal Ions in Biological Systems*, Vol. 11, Sigel, H., Ed.; Dekker: New York, 1980; p 1.
(11) Slater, J. C. *The Self-Consistent Field for Molecules and Solids*; McGraw-Hill: New York, 1974.
(12) Yang, C. Y.; Rabii, S. *Phys. Rev. A* **1975**, *12*, 362.
(13) (a) Yang, C. Y.; Case, D. A. In *Local Density Approximations in Quantum Chemistry and Solid State Physics*, Dahl, J., Avery, J. P., Ed.; Plenum: New York, 1984; p 643. (b) Yang, C. Y. In *Relativistic Effects in Atoms, Molecules, and Solids*, Malli, G. L., Ed.; Plenum: New York, 1983; p 335.
(14) Johnson, K. H. *J. Chem. Phys.* **1966**, *45*, 3085.
(15) Truter, M. R.; Milburn, C. W. *J. Chem. Soc. A* **1966**, 1609.
(16) Schwarz, K. *Phys. Rev. B* **1972**, 2466.
(17) (a) Katsuki, S.; Palting, P.; Huzinaga, S. *Comput. Phys. Commun.* **1978**, *14*, 13. (b) Katsuki, S.; Klobukowski, M. Ibid **1982**, *25*, 39.

TABLE II: Dirac NR ($c = \infty$) Orbital Energies and Charge Distributions for *cis*-DDP

		Pt			2Cl		2N		$2H_{ax}$	$4H_{eq}$
level[a]	$-E$,[b] eV	6s	6p	5d	3s	3p	2s	2p	1s	1s
$4b_2$*	2.2327	0.0	46.2	0.0	0.0	27.6	0.0	20.2	0.0	6.0
$9a_1$*	2.2819	4.7	1.0	6.8	1.4	22.8	32.6	1.6	8.6	20.5
$7b_1$*	2.9910	0.0	0.0	48.1	0.9	27.2	7.0	11.6	1.6	3.6
$8a_1$	6.5046	0.1	0.0	46.4	0.0	45.2	0.0	4.8	2.6	0.8
$3a_2$	6.6453	0.0	0.0	31.3	0.0	62.6	0.0	4.2	0.0	2.0
$3b_2$	6.7238	0.0	0.3	37.6	0.0	50.4	0.0	7.8	0.0	3.6
$7a_1$	6.8343	16.6	2.2	27.5	0.2	46.8	0.2	4.8	1.2	0.8
$6b_1$	7.2698	0.0	0.6	0.7	0.0	93.4	0.6	4.0	0.0	0.7
$6a_1$	7.5547	4.1	3.2	38.7	0.0	19.2	1.6	26.4	0.2	6.8
$5b_1$	7.7056	0.0	8.6	5.1	0.2	52.2	1.4	26.4	6.0	0.0
$5a_1$	8.0081	0.0	0.0	33.8	0.0	28.4	0.0	27.2	0.0	10.4
$2b_2$	8.3115	0.0	2.1	34.3	0.0	40.0	0.0	17.2	0.0	6.4
$2a_2$	8.3282	0.1	6.6	15.8	0.2	52.2	0.2	19.0	5.6	0.0
$4b_1$	8.9575	0.0	2.5	1.0	0.2	9.4	0.0	67.2	10.8	9.2
$1a_2$	9.6236	0.0	0.0	38.2	0.0	3.3	0.0	47.0	0.0	11.6
$1b_2$	9.7393	0.0	0.6	32.5	0.0	1.2	0.0	52.2	0.0	13.2
$4a_1$	10.1837	0.1	0.1	37.8	0.0	6.8	0.0	45.0	6.2	4.0
$3a_1$	10.4097	7.3	1.5	29.8	0.6	6.6	0.2	45.4	3.6	4.8
$3b_1$	10.9408	0.0	1.1	45.2	0.8	6.6	0.0	39.2	2.2	5.2

[a] The highest occupied orbital is $8a_1$ with charge distributions 34% d_{z^2} and 12.4% $d_{x^2-y^2}$. [b] The lower energy orbitals (eV) are −20.0928 ($1a_1$, 77% N 2s; 9.4% Cl 3s; 5% H 1s; 4% Pt 6s), −19.9194 ($1b_1$, 84% N 2s; 6% Pt 5d; 5% H 1s), −19.4226 ($2a_1$, 87% Cl 3s; 9% N 2s), and −19.3378 ($2b_1$, 95% Cl 3s).

TABLE III: Dirac Total Valence Populations (Units of Electrons/Atom) for DSW Calculations and DNR ($c = \infty$) Calculations

l	j	Pt	Cl	N	H_{ax}	H_{eq}
			A. DSW			
s	$^1/_2$	0.920	1.953	1.743	0.430	0.446
p	$^1/_2$	0.311 } 1.55[a]	1.713 } 2.03	1.467 } 1.97		
	$^3/_2$	0.482 }	3.478 }	2.901 }		
total p		0.793	5.191	4.368		
d	$^3/_2$	3.823 } 1.38				
	$^5/_2$	5.310 }				
total d		9.133				
total atom		10.846	7.144	6.111	0.430	0.446
			B. DNR			
s	$^1/_2$	0.649	1.954	1.752	0.435	0.452
p	$^1/_2$	0.235 } 2.00	1.749 } 2.00	1.460 } 2.00		
	$^3/_2$	0.469 }	3.497 }	2.919 }		
total p		0.704	5.246	4.379		
d	$^3/_2$	3.723 } 1.50				
	$^5/_2$	5.585 }				
total d		9.308				
total atom		10.661	7.200	6.131	0.435	0.452

[a] Ratio of $j = l + {}^1/_2$ to $j = l - {}^1/_2$ populations.

of calculations we have employed the Case and Karplus partitioning scheme[18] to assign the charge in the intersphere region to real atoms.

The results for the relativistic DSW method is given in Table I, whereas the $c = \infty$ classical limit (DNR) is written in Table II. A relativistic analysis of the total valence populations for *cis*-$[Pt(NH_3)_2Cl_2]$ and its $c = \infty$ limit is shown in Table III, while the Pauli decomposition for those orbitals having metal contribution mainly is given in Table IV. Moreover, Table V shows transition state (TS) calculations of spectral properties for the DSW results, and, finally, Table VI gives the results obtained for the Schrödinger MSWX_α method where ligand contributions to each MO are analyzed in terms of $\sigma - \pi$ ($D_{\infty h}$) contributions from N_2 and Cl_2 molecules in the platinum complex compound *cis*-$[PtCl_2N_2H_6]$.

III. Ground-State Results

Valence molecular orbital energies for *cis*-DDP are shown in Figure 2 for the DSW method, for its DNR ($c = \infty$) limit, and for the Schrödinger MSW method. For all these methods we find that some common features are apparent. For example, the HOMO levels are mainly 5d metal character for both the Dirac and Schrödinger approaches and, despite the fact that Dirac equation and Schrödinger equation are solved independently, the close agreement between both methods is remarkable. In fact, the ordering of energy levels is almost the same when comparing the Schrödinger results to the DNR ($c = \infty$) results since here l is still a good quantum number. Upon inclusion of relativity we see that the relative splittings between levels containing significant 5d-metal character increase greatly, e.g., $1a_2 \rightarrow 1b_2$ (NR, 0.11 to 0.20 eV), $4a_1$ states), $3a_1$ (NR, 0.22 to 0.68 eV), $8a_1 \rightarrow 3a_2$ (NR, 0.14 to 0.47 eV), and $2b_2 \rightarrow 2a_2$ (NR, 0.02 to 0.2 eV), due to the extra occupation introduced by spin–orbit mixings (since the NR orbitals are pure spin states), thereby giving rise to different charge distributions under different calculation schemes. Furthermore, it is well-known that relativistic effects tend to destabilize d orbitals and to stabilize the metal–ligand interactions so that relativistic corrections are quite important for platinum complex molecules.[13] The molecular orbital system shown in Table I allows us to divide the valence set of orbitals into three well-defined groups of orbitals, namely, the unoccupied 5d(Pt)–π* (ligand) and 6p(Pt)–π* (ligand) orbitals, the occupied molecular orbitals supporting the complex molecule, and the inner localized 2s(N) and 3s(Cl) orbitals at ~−20 eV. For the latter, Schrödinger results are lower in energy than the equivalent DNR ($c = \infty$) energies. It is also interesting to realize that the NH_3 molecule does not have localized MOs except for the $1a_1$ and $1b_1$ inner orbitals. Furthermore, 2p(N) functions appear delocalized in most

(18) Case, D. A.; Karplus, M. *Chem. Phys. Lett.* **1976**, *39*, 33.

TABLE IV: Pauli Decomposition for Orbitals with Mainly Metal Character and Large Spin–Orbit Mixing

atom	*l* spin	5e	11e	12e	18e	19e	20e[a]
Pt	s β	0.001 96	0.000 98	0.058 92	0.003 59	0.013 86	0.000 04
	p α	0.014 11	0.010 65	0.008 83	0.002 69	0.000 66	0.000 26
	p β	0.000 79	0.066 18	0.018 77	0.000 02	0.000 78	0.000 02
	d α	0.398 56	0.085 51	0.153 06	0.265 81	0.101 75	0.129 57
	d β	0.032 88	0.112 62	0.132 62	0.206 71	0.381 91	0.502 47
	total α	0.412 67	0.096 16	0.161 89	0.268 50	0.102 41	0.129 83
	total β	0.035 63	0.179 78	0.210 31	0.210 32	0.396 55	0.502 53
2Cl	s α	0.006 00	0.000 04	0.000 00	0.000 00	0.000 00	0.000 00
	s β	0.000 06	0.002 78	0.001 90	0.000 00	0.000 00	0.000 00
	p α	0.053 00	0.087 16	0.189 84	0.249 24	0.077 84	0.050 62
	p β	0.002 04	0.395 76	0.231 00	0.172 68	0.347 46	0.223 40
	total α	0.059 00	0.087 20	0.189 84	0.249 24	0.077 84	0.050 62
	total β	0.002 10	0.398 54	0.232 90	0.172 68	0.347 54	0.223 40
2N	s α	0.000 34	0.000 50	0.000 00	0.000 02	0.000 02	0.000 04
	s β	0.000 00	0.002 66	0.000 74	0.000 42	0.000 00	0.000 14
	p α	0.396 36	0.060 20	0.063 88	0.042 88	0.015 88	0.013 38
	p β	0.018 70	0.122 22	0.086 18	0.021 90	0.033 74	0.042 56
	total α	0.396 70	0.060 70	0.063 88	0.042 90	0.015 90	0.013 42
	total β	0.018 70	0.124 88	0.086 92	0.022 32	0.033 74	0.042 70
$2H_{ax}$	s α	0.020 38	0.006 34	0.000 02	0.000 00	0.000 00	0.000 00
	s β	0.003 24	0.031 70	0.005 20	0.008 50	0.001 42	0.016 70
$4H_{eq}$	s α	0.051 48	0.012 96	0.023 92	0.021 04	0.008 00	0.007 56
	s β	0.000 12	0.001 79	0.025 16	0.004 52	0.016 60	0.013 20

[a] HOMO level.

TABLE V: Ionization Energies (eV) and Transition (TS) Energies (μm^{-1}) for *cis*-DDP

	$(-\epsilon_k - 2.07)$	expt
Ionization Energy		
		24.1[a]
2e → vacuum	17.96	
4e → vacuum	17.50	17.1
5e → vacuum	8.84	8.7
15e → vacuum	5.50	6.0
18e → vacuum	4.45	
19e → vacuum	4.39	
20e → vacuum	3.92	4.0
Transition Energy		
20e → 21e	2.77	2.7[b]
20e → 22e	3.24	
20e → 23e	3.28	
19e → 21e	3.15	3.25
19e → 22e	3.57	
19e → 23e	3.61	3.55

[a] Taken from ref 4. [b] Values obtained from ref 6 and 22.

of the MOs in the valence energy region with the exception of the four highest occupied orbitals for which chlorine and platinum contribute most.

In addition to this, it is interesting to compare the charge supported by the metal orbitals under the different methods of calculations. It is seen that both DSW and its DNR ($c = \infty$) results predict a $5d^{9.1}$ and a $5d^{9.3}$ (see Table III) orbital population, respectively, whereas Schrödinger results yield a $5d^{9.2}$ electronic population in spite of the fact that differences exist for the percentage of charge distributed among the calculated levels. Furthermore, there are small (6s/6p) admixtures in the occupied valence levels probably through ligand-donation charge-transfer processes. Relativistic effects play an important role in this matter because the energy change when passing from full relativistic DSW results to Schrödinger results also changes the energy position of the starting orbitals, and the numerical values for the charge distributions given in Table I, II, and VI are different. The DSW (and its DNR ($c = \infty$) limit) lowest energy excited orbital is of mainly Pt(5d) character. This is an important result for *cis*-DDP since recent DSW calculations[30] on square-planar PtX_4^{2-} complexes show that the LUMO level is ligand dependent, i.e., for weak field ligands (x = Cl and Br) the LUMOs consist of almost equal admixtures of Pt(5d) and ligand orbitals, whereas for strong field ligands (X = CN^-) the LUMO consists of mostly equal

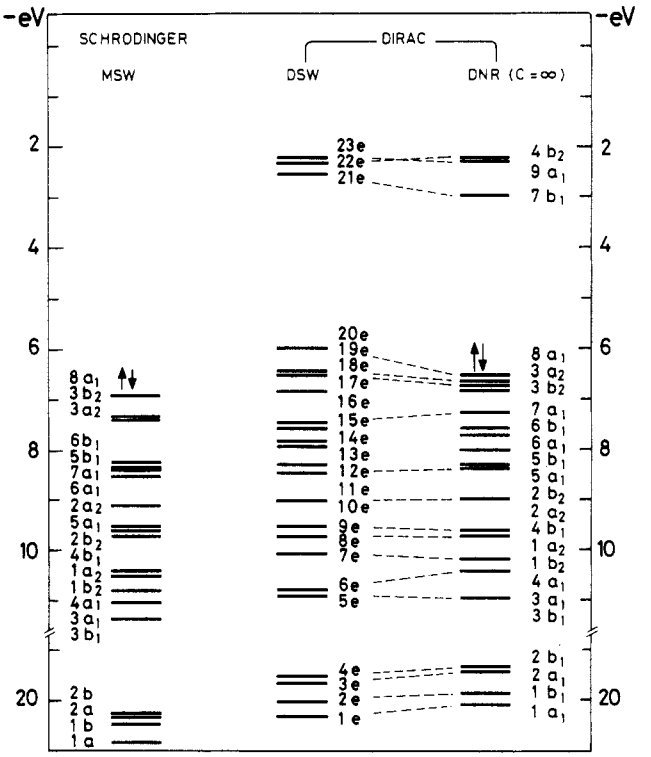

Figure 2. Valence energy level diagram for *cis*-DDP. The highest doubly occupied HOMO level for each Schrödinger and Dirac ($c = \infty$) are shown explicitly. The HOMO (DSW) is 20e and double group notation is used, e (or γ_5) orbitals are twofold degenerate.

Pt(6p) and ligand contributions. These observations are borne out by other Schrödinger scattered wave calculations on $[Pt(PH_3)_2O_2]$ and $[Pt(CN)_4]^{2-}$ complexes, where the LUMOs are of 6p(Pt) nature.[19,20] Moreover, preliminary DSW results for $Pt(en)Cl_2$ also reveal that the LUMO is made of ligand and 6p(Pt) functions. For the case under study, Schrödinger calculations for *cis*-DDP yield a LUMO level of 6p(Pt) and ligand admixtures and this is indicative of the better MO picture offered by full relativistic calculations for this platinum complex molecule, though

(19) Norman, J. G. *J. Am. Chem. Soc.* **1974**, *96*, 3327.
(20) Interrante, L. V.; Messmer, R. P. *Chem. Phys. Lett.* **1974**, *26*, 225.

TABLE VI: Schrödinger MSW Energy Levels and Valence Orbital Populations[a] for *cis*-$[Pt(Cl_2)(N_2)(H_6)]$

$-E$, eV	Pt				N_2			Cl_2			H_6	
a_1	s	p_z	d_{z^2}	$d_{x^2-y^2}$	$\sigma_g(s)$	$\sigma_g(x)$	$\pi_u(z)$	$\sigma_g(s)$	$\sigma_g(x)$	$\pi_u(x)$	2 ax	4 eq
6.909			47	17		9	9		8	7	1	2
8.399	23	6	3	13	1	2	31			39	2	
8.508	3		10	28		5	1		2	30		1
9.570		9				27			59	1		4
10.815	7		19	16		27	11	1	12	3	1	2
10.032			22	21		8	29		3	13	1	2
a_2	d_{xy}				$\pi_g(y)$			$\pi_g(y)$				4 eq
7.390	55				18			25				2
9.050	3				32			62				3
10.401	47				40			11				2
b_1	p_x	d_{xz}			$\sigma_u(s)$	$\sigma_u(x)$	$\pi_g(z)$	$\sigma_u(s)$	$\sigma_u(x)$	$\pi_g(z)$	2 ax	4 eq
8.170	5	1			1	9	4	78		1		1
8.302	2				47		11		1	33		6
9.680	8	1			7		37			42	3	2
11.334	1	47			16		21	1	6	5	2	1
b_2	p_y	d_{yz}			$\pi_u(y)$			$\pi_u(y)$				4 eq
7.371		55			18			25				2
9.566	5	8			18			67				2
10.473	1	40			50			6				3

[a] The doubly degenerate π diatomic functions ($D_{\infty h}$) are written under the corresponding irrep of C_{2v}.

both schemes of calculations yields similar ground-state results overall.

It should be pointed out that neither DSW results nor Schrödinger SW results given here agree with the previous Schrödinger MSW X_α calculations of Barber et al.[4] For example, their HOMO level is of ligand localized nature for an identical geometry[15] in the tangent sphere formalism. It is probable that their results are in error since, experimentally,[7,22] the HOMO level is of metal d nature.

Relativistic Effects. Surprising results are seen from the values given in Table III. To begin with, the ratio between $j = l - {}^1/_2$ and $l + {}^1/_2$ components for the d metal levels yield slightly different results for both cases DSW and its DNR ($c = \infty$) limit. These findings are reflected in Figure 2 where energy displacements when passing from fully relativistic DSW to DNR ($c = \infty$) are not pronounced ($\sim$0.5 eV). However, that ratio for 6p(Pt) electrons differs appreciably (1.55 ratio for DSW against 2.00 ratio for DNR ($c = \infty$)), whereas chlorine and nitrogen yield similar results fo r both population ratios. Thus, platinum 6p functions are important to account for relativistic effects in *cis*-DDP. They accept 0.79 electrons probably due to hydrogen donation through Pt–N interactions.

Table IV gives the Pauli decomposition for those orbitals showing large contributions from the metal atoms. The values have been calculated in terms of the two DSW large components only and it has been assumed that the radial wave function is the same for both of them. In the nonrelativistic limit (not shown) pure spin states are obtained and a measure of the extent of spin–orbit mixings is given by the amount of minority spin mixed into the relativistic orbital. Within the platinum sphere, this contamination is always significant, except for the 5e level, for which the minority spin is 8.5% of the majority spin, whereas in the 19e and 20e (HOMO) levels the minority spins are 26% of the majority spins. The character of these spin–orbit mixings are $d_{z^2}\ \beta$, $d_{yz}\ \alpha$, and $d_{xz}\ \alpha$, respectively. Notwithstanding energy displacements between DNR ($c = \infty$) and DSW, results are rather small; we find that spin–orbit mixings in the molecular spinors are significant and Pt is its greatest contributor. Thus, increasing metal–ligand bonding is easily deduced from a close examination of the relativistic 5e orbital of Table I and it is clear that relativistic effects will make difficult the analysis of spectral data in terms of ligand field parametrization.

The values given in Tables I and II show that 5d(Pt) and 3p(Cl) contribute significantly to the highest three occupied MOs mixed with relatively small contributions from 2p(N) functions. The HOMO level consists of d_{z^2} and $d_{x^2-y^2}$ character according to the Cartesian axes of Figure 1 and either Schrödinger or Dirac ($c = \infty$) calculations give a >34% contribution of d_{z^2} for the charge distribution of that level. The energy ordering established for d orbitals in the three highest occupied MOs is $d_{z^2} > d_{yz} > d_{xy}$ for the DNR ($c = \infty$) limit, though none of them is a pure metal orbital. Furthermore, the established ordering also holds for the Schrödinger results of Table VI so that we can state with confidence that both methods of calculations yield consistent results.

This consistency is not seen when other calculations for *cis*-DDP are analyzed. Thus, Carsey et al.[5] applied the extended Hückel method to include relativistic corrections for platinum exclusively and found that the HOMO level is of ligand nature mainly, with some 6s(Pt) character and little 5d(Pt) character, whereas their extended Hückel nonrelativistic results assign a 55.8% 5d(Pt) character to the HOMO level. Moreover, their HOMO/LUMO energy gap is 6.2 eV for the nonrelativistic EH results and it decreases to 0.28 eV when relativistic effects are included. Obviously, these inconsistencies are due to the extreme parametrization of the extended Hückel method.

The difference in ordering observed for the virtual levels from DSW and DNR ($c = \infty$) given in Tables I and II deserves some comments. To begin with, the third highest DNR ($c = \infty$) orbital is mainly 6p(Pt) character whereas the equivalent one from DSW consists mainly of 2s(N) character. However, this is an expected result since relativistic effects stabilize the 6p(Pt) orbital whereas relativistic effects over 2s(N) are negligible. Overall, as summarized in Tables I and II, the MO description presented for *cis*-DDP seems appropriate to learn more about its bonding properties.

The high spin–orbit contaminations shown in Table IV associated with the nonlocalized nature of the MOs involved indicate that attempts to assign electronic transition based on nonrelativistic grounds should be definitely disclosed for *cis*-DDP, and this includes d–d transitions and charge-transfer transitions. In fact, it is easily seen from Figure 2 and Tables I and II that, for example, the DNR ($c = \infty$) b_1* level moves 0.436 eV (0.34 μm^{-1}) to higher energies due to relativistic effects over its mainly d_{xz}(Pt) character, whereas a_1* and b_2* of ligand and 6p(Pt) character, respectively, do not show energy displacements to the same extent. These features are also observed for the highest occupied levels for *cis*-DDP and are of the same nature as those calculated for the $PtCl_4^{2-}$ molecule.[21] Thus, it is natural to expect that electronic spectral assignments based on DSW methods should be more reliable. Furthermore, due to the spin-restricted nature of the method, this does not distinguish between singlet and triplet states

(21) Larsson, S.; Olsson, L. *Int. J. Quantum Chem.* **1984**, *25*, 201.
(22) Chatt, J.; Gamlen, G. A.; Orgel, L. E. *J. Chem. Soc.* **1958**, 486.

though an emphasis on approximate methods of including spin polarization effects in relativistic calculations have been discussed.[32]

In keeping with these objectives, the TS calculations for the 20e → 21e electronic transition yields the 2.77-μm^{-1} value, in excellent agreement with the 2.7-μm^{-1} experimental value.[6] This is the lowest energy electronic transition from DSW calculation, it is of d–d type mainly, it involves the $5d_{5/2}$ component, and it is highly spin contaminated. The spatial d orbitals involved are $d_{z^2} \rightarrow d_{xz}$ mainly according to the Cartesian axis shown in Figure 1. Moreover, the excitation is delocalized over the Cl_2 and the N_2 molecular species along σ(Px) and π(Pz) components, respectively. It is a molecular electronic promotion delocalized over the square-planar arrangement of atoms for the complex.

The next observed band at 3.25 μm^{-1} cannot be assigned to a single orbital change as before. Actually, Table V shows that the 20e → 22e ($5d_{5/2}$ → 6p; ligand), the 20e → 23e (5d → ligand), and the 19e → 21e (d–d) transitions contribute to its intensity where the last d–d electronic promotion lies at the lower energy side of the band. Thus, the observed higher intensity of that adsorption band is due to 5d → 6p intrametal and 5d → ligand charge-transfer transition and it should not correspond to a pure d–d type promotion.

There is also another peak measured at 3.5 μm^{-1} of comparable intensity to that just described and it agrees rather well with the calculated values for the 19e → 22e (5d → 6p; ligand) and 19e → 23e (d → L) orbital changes. It is remarkable that this band, theoretically, does not have d–d components. For the purpose of completeness, let us say that the strong charge-transfer bands observed at 4.65 μm^{-1} and higher are not a matter of discussion so that we have not included calculations for them. Probably, a simple orbital energy difference explains rather well their origin starting from the 17e orbital to any of the vacant orbitals. Instead, let us say that it is clear now that Dirac relativistic results are necessary for the proper assignments of electronic transitions for *cis*-DDP, and metal localized orbitals do not provide good mechanisms for electronic excitations; the same could be said with respect to Schrödinger X_α results for *cis*-DDP.

Ionization energies are also given in Table V for the DSW tangent sphere approach. Before discussing the results, let us put forward several comments. First, ionization energies in the scattered wave technique with tangent spheres are usually higher than the experimental values and second, the use of overlapping spheres normally corrects the discrepancies in the right sense without justifying the method employed.[23] An alternative approach[24] is to realize that the ionization potential (IP) for a given orbital k is approximately given by $IP \simeq -\epsilon_k + {}^1/_2(J_{kk} - I_{kk})$ where J_{kk} is the usual Coulomb integral and I_{kk} arises from the correction to the statistical local exchange term because of the electron density change $\langle \rho(r) - |\psi_k(r)|^2 \rangle^{1/3}$ due to ionization of an electron in the orbital ψ_k. Moreover, I_{kk} is a small term compared to J_{kk} so that the correction to $-\epsilon_k$ is large, of the order ${}^1/_2 J_{kk}$. Finally, the statistical nature of the X_α formalism suggests that a good method to properly assign ionization potentials is to estimate an average correction for all levels $-\epsilon_k$ for any k by using well-fitted results from experiments. The ESCA data given in Table V are easily understood if an average difference of 2.07 eV between the DSW calculation and the experimental results is accepted. Thus, the peak observed at 17 eV refers to a set of orbitals localized on the Cl and N moieties mainly. If we consider a Pt–Cl_2 bond and take Cl_2 as a molecular species we deduce that this peak arises from the ionization of σ_g(3s) and σ_u(3s) MOs which, for the normal chlorine molecule,[25] appears at ~23.05 eV. However, the greater Cl–Cl distance and different charge distribution in *cis*-DDP for that molecule results in a lower value for this peak. A similar analysis could be performed for the other peaks and we find that the observed band at ~8.7 eV arises from the ionization of $3\sigma(N_2)$ and $1\pi(N_2)$ electrons whereas the peak at ~6.0 eV arises from the ionization of electrons from σ and π orbitals made of 3p chlorine functions mainly. Finally, the ESCA peak at ~4.0 eV correlates rather well to the higher energy orbitals 17e up to 20e, all of them being composed of almost equal contribution of both Pt(5d) functions and $Cl_2(\pi)$ functions as described in Table VI. Thus, our analysis either by DSW or Schrödinger MSW methods allows us to fit rather well experimental ionization energies, in contradiction to previous statement[4] about X_α methods for this molecule.

IV. Bonding Properties

An interesting bonding scheme for *cis*-DDP arises from the MO calculations performed here. The nature of the metal–ligand interactions induces large charge-transfer among all the atoms in the molecule as is easily seen from Tables III and IV. The result is that Pt and N have acquired approximately one electron each at the expense of the highly positive charge supported by hydrogens. The DSW results show that the charge formula is $[Pt^{-0.85}(N^{-1.11})_2(Cl^{-0.14})_2(H_{ax}{}^{+0.57})_2(H_{eq}{}^{+0.55})_4]$ which compares rather well to both the DNR ($c = \infty$) limit result $[Pt^{-0.66}(N^{-1.13})_2(Cl^{-0.2})_2(H_{ax}{}^{+0.57})_2(H_{eq}{}^{+0.55})_4]$ and to the Schrödinger result $[Pt^{-0.99}(N^{-1.72})_2(Cl^{-0.26})_2(H_{ax}{}^{+0.87})_2(H_{eq}{}^{+0.81})_4]$. All of them show that the molecule depicted in Figure 1 has a (+) region of hydrogen atoms and a (−) region delocalized over the square-planar arrangement of Pt, Cl, and N atoms. Obviously, the differences between Schrödinger and Dirac results are due to general features of relativistic compared to nonrelativistic eigenvalues; especially contraction of 6s(Pt) and 6p(Pt) shells and expansion of 5d(Pt) shells. These facts produce slightly different charge distributions of the atoms involved. However, both Schrödinger and Dirac bonding schemes for *cis*-DDP predict that a large amount of charge (3.34 e^-) flows from H atoms to the (Pt, Cl, N) skeleton and a close comparison between both schemes reveals that gross charge transfer is not substantially affected by relativistic effects.

The results given in Table II show that 5d(Pt) orbitals play an important role in the bonding scheme starting from the $3b_1$ bonding orbital at −10.94 eV up to $8a_1$ nonbonding orbital at −6.50 eV. Furthermore, L → 5d(Pt) donation exists in slight amounts compared to L → 6p(Pt). In fact, Table III shows that 6p(Pt) has got 0.79 e^- from ligands (mainly from the Hs) whereas only 0.13e^- have migrated to 5d(Pt). These results confirm a recent statement[9] about the role of metal p orbitals in the bonding for complex molecules from heavy metals. They allow important mixings between different sets of ligand orbitals to provide mechanisms for charge migration.

Another important feature to realize is that hydrogen functions do not contribute appreciably to the bonding scheme for *cis*-DDP. To the contrary, there is a diatomic N_2 molecule of (−) charge and a hydrogen cloud of (+) charge at one end of the square plane, and a Cl_2 molecule of (−) charge at the other end. This bonding picture is supported by the contour maps of Figure 3 for the (xz) square-planar projection of the relativistic two large components ψ_1 and ψ_2 for the HOMO (20e) and LUMO (21e) levels. Here ψ_1 is the minor component for each case and gives information about spin–orbit mixings which is antibonding among all real atoms. The major component ψ_2 (spin down) should be virtually identical with the nonrelativistic orbital; thereby the net bonding properties are mainly given by this component. Thus, it is seen in Figure 3 that ψ_2 (20e) for the HOMO level shows the existence of a Cl–Cl (upper atoms) bonding region of (−) sign and also a N–Cl bonding region of (+) sign. Moreover, both N atoms (lower atoms) are antibonding among them and the platinum d_{z^2} and $d_{x^2-y^2}$ functions are in opposite phases to the ligand orbitals so that there is no net Pt–ligand bond present in this HOMO level.

Different results are observed for the LUMO (21e) level; here the minor component is ψ_2 (spin down), where one finds now a N–N bonding region together with a N–Cl bond of opposite phase and a nonbonding region between the Cl atoms. Again this ψ_2 component (which transforms as $a_1\beta$ in C_{2v}) is not bonding at all between Pt and ligands. The major ψ_1 component, which in Pauli description transforms as Im ($b_1\alpha$), shows no net metal–ligand bond.

(23) Case, D. *Annu. Rev. Phys. Chem.* **1982**, *33*, 151.
(24) Trsic, M.; Laidlaw, W. G. *Int. J. Quantum Chem.* **1983**, *S7*, 367.
(25) Dycke, M.; Josland, G. D.; Snijders, J. G.; Boerrigter, P. M. *Chem. Phys.* **1984**, *91*, 419.

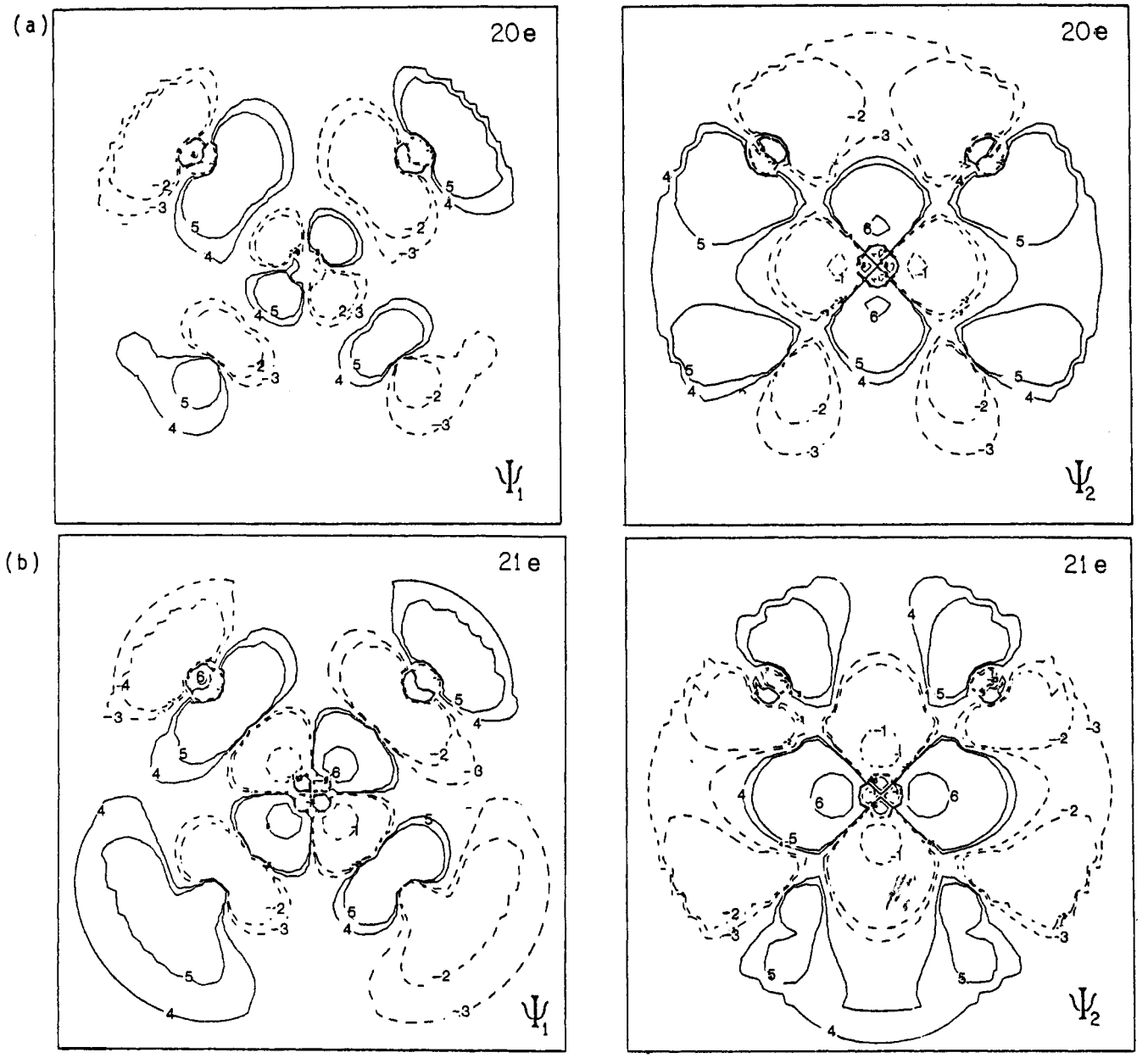

Figure 3. (a) Contours of the ψ_1 and ψ_2 large components of the HOMO (20e) level obtained in the DSW calculation for *cis*-DDP. Contour values (in electron/bohr^3)$^{1/2}$ are (1,6), (2,5), (3,4) = ±0.02, ±0.002, ±0.0002 for ψ_1; and ±0.200, ±0.020, ±0.002, for ψ_2. The upper atoms are Cl and the lower atoms are N. (b) Contours of the ψ_1 and ψ_2 large components of the LUMO level. Contours of the ψ_1 component of the LUMO (21e) are equivalent to the ψ_2 (20e) component, while the contours of ψ_2 (21e) correspond to the ψ_1 (20e) component, as specified above.

These findings suggest that a suitable model to study bonding phenomena for *cis*-DDP is to formulate it as *cis*-$[Pt(Cl_2)(N_2)(H_6)]$ to make use of the σ and π descriptions for the diatomic molecules. The Schrödinger results for this complex system is given in Table VI for each irrep of C_{2v} and Figure 4 shows its MO diagram with the calculated X_α energies for the Cl_2 and N_2 isolated molecules at the interatomic distances found in *cis*-DDP. These results show that the $\sigma_u^*(2p)$ and $\pi_g^*(2p)$ diatomic unoccupied orbitals for the isolated N_2 molecule have 5 e^- when in *cis*-DDP, distributed mostly in $5b_1$, $4b_1$, and $3b_1$ (with $\pi_g^*(p_z)$ and σ_u^*) and in $3a_2$, $2a_2$, and $1a_2$ (with $\pi_g^*(p_y)$). Similar results are found for the chlorine molecule for which we can write its MO description in *cis*-DDP as $Cl_2[(3\sigma_g)^{2.0}(3\sigma_u)^{2.0}(4\sigma_g)^{1.7}(2\pi_u)^{3.7}(2\pi_g)^{3.5}(4\sigma_u^*)^{1.7}]$ so that 1.7 e^- are located in $4\sigma_u^*$, whereas this orbital was empty in the Cl_2 isolated molecule. Moveover, for the nitrogen molecule we find $N_2[(2\sigma_g)^{1.8}(2\sigma_u)^{1.7}(3\sigma_g)^{1.6}(1\pi_u)^{3.3}(1\pi_g^*)^{3.3}(3\sigma_u^*)^{1.7}]$. Obviously, the excess of charge for each diatomic molecule in *cis*-DDP is provided by the hydrogen atoms.

Let us focus our attention into the 5d(Pt) orbitals for the Cartesian axis shown in Figure 1. For example, we find from Table VI that the metal $(5d)^{9.2}$ electron configuration is actually close to $5d[(z^2)^{2.0}(x^2-y^2)^{2.0}(xy)^{2.0}(yz)^{2.0}(xz)^{1.2}]$, that is, only the $5d_{xz}$ directed toward ligands is not fully occupied, indicating that the MO description given here is essentially correct, within the restriction imposed by the Case and Karplus[18] algorithm to assign the charge in the intersphere region to real atoms. In the same manner, it is found that the metal $(6p)^{0.9}$ configuration can be written $6p[x^{0.4}y^{0.1}z^{0.4}]$, so that most of the charge arises from the molecular plane around the Cl–Cl bond and N–Cl bond.

Molecular Electronegativity χ. It is well established in the literature[26] that the electronic chemical potential μ of density functional theory equals the negative of the absolute electronegativity χ which, in principle, is evaluated by means of the X_α orbital energies for atoms[27] and molecules.[28] It is also well-known that χ is identified $\chi = -\epsilon_{HOMO}$ for open-shell molecules, whereas both HOMO and LUMO orbital energies are needed for closed-shell

(26) (a) Parr, R. G.; Donnelly, R. A.; Levy, M.; Palke, W. E. *J. Chem. Phys.* **1978**, *68*, 3801. (b) Parr, R. G. *Annu. Rev. Phys. Chem.* **1983**, *34*, 631.
(27) (a) Bartolloti, L. J.; Gadre, S. R.; Parr, R. G. *J. Am. Chem. Soc.* **1980**, *102*, 2945. (b) Robles, J.; Bartolloti, L. J. *J. Am. Chem. Soc.* **1984**, *106*, 3723.
(28) Vera, L.; Zuloaga, F. *J. Phys. Chem.* **1984**, *88*, 6415.

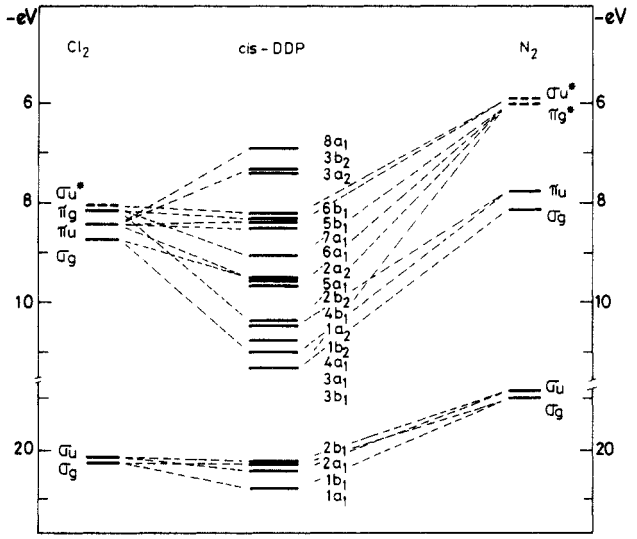

Figure 4. Schrödinger valence molecular orbital diagram for *cis*-$[PtN_2Cl_2H_6]$ in terms of diatomic molecules. The H atoms are not shown explicitly.

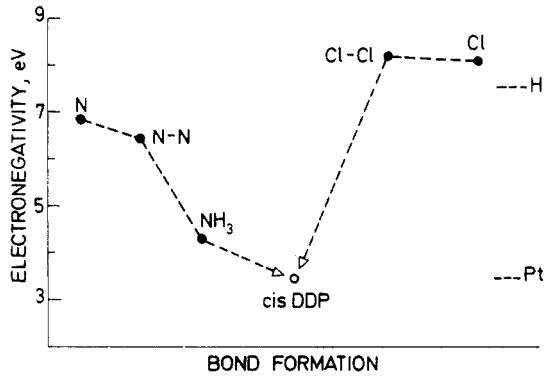

Figure 5. Atomic and molecular electronegativity diagram for *cis*-DDP formation. Interatomic distances (in bohr) are 6.227 (Cl–Cl) and 5.372 (N–N).

molecules. In general, the molecular geometry plays a fundamental role to fix the χ value.[28]

In Figure 5 the molecular electronegativity for *cis*-DDP is presented together with the Schrödinger χ values for its free ligands. The diatomic species were calculated by using tangent spheres whereas the electronegativity for NH_3 was deduced from literature data.[33] Obviously, the value χ = 3.421 eV for *cis*-DDP arises from DSW orbital energies and is 0.46 eV lower than the DNR ($c = \infty$) value for this platinum complex molecule.

Let us take a closer look at the trends observed in Figure 5. To begin with, the free N_2 molecule at d(N–N) = 5.372 bohr (found in *cis*-DDP) is a lower electronegativity species in comparison to its free atom constituents and this behavior is not seen for the free chlorine molecule at d(Cl–Cl) = 6.227 bohr (found in *cis*-DDP). However, the free NH_3 molecule becomes a lower electronegativity species that acquires the 3.421-eV value when in the complex molecule. Furthermore, the situation for Cl_2 is rather different since, for this case, it is striking that the value $\chi(Cl_2)$ = 8.234 eV is strongly decreased to the common value in the complex because of back-donation to its σ_u* orbital (see Figure 4). It is also remarkable how close the molecular electronegativity for *cis*-DDP lies to the free Pt χ = 3.44-eV value, a rather low value in reference[27] to those for Cl, N, and H. This last fact seems to hold true for square-planar complexes.[28] Thus, platinum plays the remarkable role of modulating the molecular reactive capacity of *cis*-DDP and this includes all the atoms (or molecular species) in the complex.

V. Conclusions

We have presented here a detailed MSW study of the electronic structure of *cis*-$[Pt(NH_3)_2Cl_2]$. The relativistic (Dirac) calculations (including Darwin, mass velocity, and spin–orbit corrections at the SCF stage) in the four-component scheme reveals that relativistic effects increase the nonrelativistic splitting of the levels containing 5d metal character. Moreover, the Pauli decomposition for the MOs showing large contributions from the Pt atom suggests that spin contaminations are significant and make difficult the analysis of spectral data, unless one uses relativistic methods for its MO description. The established molecular orbitals show that L → 5d(Pt) donation is low in comparison to L → 6p(Pt) donation and suggest that metal p orbitals play an important role in the bonding scheme for *cis*-DDP.

Contour plots for the HOMO level show that Cl–Cl bonding and N–Cl bonding exist for this molecule and by assuming that its MO description could be given in terms of diatomic ligand molecules, we find that an almost neutral Cl_2 molecule exists in the complex. However, its free chlorine molecular electronegativity is drastically reduced and the Pt atom is responsible for this effect.

Passing beyond the topics discussed here, we hope that these results can be of help in understanding the nature of the molecular orbitals involved in square-planar platinum complex and in constructing working interpretations of their chemical and biological properties,[29] especially when forming part of large molecular systems.

Acknowledgment. We thank Cary Y. Yang for many useful discussions. F.Z. acknowledges financial support from FNC (674/83) for part of this work.

Registry No. *cis*-$[Pt(NH_3)_2Cl_2]$, 15663-27-1.

(29) Cleare, M. J.; Aydes, P. C.; Malerhi, B. W.; Watkins, D. M. *Biochemie* **1978**, *60*, 835.
(30) Arratia-Pérez, R.; López, J. P.; Case, D. A.; Yang, C. Y., unpublished results.
(31) Messmer, R. P.; Interrante, L. V.; Johnson, K. H. *J. Am. Chem. Soc.* **1974**, *96*, 3847.
(32) López, J. P.; Case, D. A. *J. Chem. Phys.* **1984**, *81*, 4554.
(33) Goursot, A.; Penigault, E.; Weber, J. *Chem. Phys.* **1979**, *38*, 11.

Analysis of Infrared Specular Reflection Spectroscopy for Rare Gas Matrices

J. Pacansky* and C. D. England

IBM Research Laboratory, San Jose, California 95193 *(Received: September 30, 1985; In Final Form: January 28, 1986)*

The complex refractive indexes for Ar, Kr, and Xe matrices containing CO, CO_2, and a mixture of CO + CO_2, respectively, were determined as a function of wavenumber. These, along with Maxwell's equations, were used to calculate infrared specular reflectance spectra and to investigate their utility for infrared spectroscopy of matrix isolated systems.

Introduction

The matrix isolation technique utilizing rare gas solids is a useful sampling method for obtaining spectroscopic information. Infrared spectroscopy has probably been the most popular analytical tool used to probe matrix isolated systems and to date is widely employed by a number of researchers. Infrared absorption spectra of rare gas matrices (RGM) are recorded in either a transmission or specular reflection mode; the former of course requires that the matrix is supported by an IR transparent substrate like CsI, NaCl, etc., while for the latter infrared radiation is reflected from a metal substrate upon which the matrix is deposited. The advantage of recording spectra in a transmission mode is that analysis is routine. The benefit of employing specular reflection techniques is a direct consequence of the metal substrate. Due to the thermal conductivity and mass of the metal substrate the quality of a matrix may be more carefully controlled during and after deposition, especially when radiation[1] or heat is applied to induce photochemistry or thermal chemistry.

In comparison to transmission infrared spectroscopy, infrared specular reflection spectroscopy, IRSRS, is a very complicated tool. In essence, almost all of the simplicity enjoyed in interpreting transmission spectra is lost with IRSRS. This is due to the combined effect of the film thickness, the angle of incidence, and the fact that the electric field must vanish at the surface of the metal substrate. All of this can be quantitatively understood and modeled, however, by using Maxwell's equations once the optical constants of the system are known. In this report we study as prototypes CO and CO_2 in Ar, Kr, and Xe by using a classical dispersion analysis to determine their complex refractive indexes as a function of wavenumber. In turn these are used to calculate infrared specular reflectance spectra under a number of experimental conditions to investigate when intensities in specular reflection spectra may be related to concentrations and hence useful as a tool for kinetic analysis.

Classical Dispersion Analysis and Reflectance Calculations

As an orientation for the optical parameters required to describe the infrared reflectivity of the vacuum–RGM–gold system consider Figure 1. The three refractive indexes are $n_1 = 1.0$ for the vacuum,

$$\hat{n}_2 = n_2 + i\kappa_2 \tag{1}$$

for the RGM, and

$$\hat{n}_3 = n_3 + i\kappa_3 \tag{2}$$

for the gold substrate. In eq 1 and 2, n_2 and n_3 are the real parts of the refractive indexes for the RGM and gold while κ_2 and κ_3 are the imaginary parts, respectively. In the calculations that follow, the angle of incidence for the infrared light is maintained at 14°, and h is the film thickness in centimeters.

As illustrated in Figure 1, a model for the reflectivity in the infrared of the vacuum–RGM–gold system requires n_2, n_3, κ_2, and κ_3 as a function of wavenumber (cm^{-1}) or wavelength (λ). The optical constants for gold have been studied in several laboratories and have been reported and tabulated by Ordal and co-workers.[2] In this form, they are not suitable for computer modeling. Therefore, n_3 and κ_3 were fit to polynomials which were a function of wavenumber. This fit is shown graphically in Figures 2 and 3 for n_3 and κ_3, respectively.

Optical Constants of RGM. The optical constants for the RGM were individually related to wavenumber through a dispersion analysis. Since the dispersion analysis is only performed on RGM, for the sake of simplicity in notation the subscript 2 will be dropped in the following discussion for the analysis. The refractive index for the RGM is cast in the form of the dielectric constant, ϵ, as

$$\epsilon = (\hat{n})^2 = \epsilon_r + i\epsilon_i \tag{3}$$

where

$$\epsilon_r = n^2 - \kappa^2 \tag{4}$$

and

$$\epsilon_i = 2n\kappa \tag{5}$$

By the use of eq 4 and 5, the following expressions for n and κ are obtained:

$$n^2 = (1/2)\{(\epsilon_r^2 + \epsilon_i^2)^{1/2} + \epsilon_r\} \tag{6}$$

$$\kappa^2 = (1/2)\{(\epsilon_r^2 + \epsilon_i^2)^{1/2} - \epsilon_r\} \tag{7}$$

The real and imaginary parts of the dielectric constant, ϵ_r and ϵ_i, were determined by using the classical dispersion analysis reported by Spitzer and Kleinman[3] and Maeda and Schatz[4] as given below

$$\epsilon_r = \epsilon_0 + \sum_{j=1}^{N} 4\pi\rho_j\nu_j^2 \frac{\nu_j^2 - \nu^2}{(\nu_j^2 - \nu^2)^2 + \gamma_j^2\nu_j^2\nu^2} \tag{8}$$

$$\epsilon_i = \sum_{j=1}^{N} 4\pi\rho_j\nu_j^2 \frac{\gamma_j\nu_j\nu}{(\nu_j^2 - \nu^2)^2 + \gamma_j^2\nu_j^2\nu^2} \tag{9}$$

where the summation is over the N oscillators in the system, ϵ_0 is the short-wavelength dielectric constant, ν_j is the frequency of the jth oscillator, γ_j is related to the full width at half height by

$$\gamma_j = \Delta\nu_{(1/2)}/\nu_j \tag{10}$$

and ρ_j is related to the integrated absorption

$$A_j = (1/h)\int_j \ln(T_0/T)\, d\nu \tag{11}$$

by

$$\rho_j = (\tilde{n}A_j)/(4\pi^3\nu_j^2) \tag{12}$$

where $\tilde{n}$ is the mean refractive index.[5]

(1) Pacansky, J.; Maier, M. *J. Phys. Chem.*, manuscript in preparation.

(2) Ordal, M. A.; Long, L. L.; Bell, R. J.; Bell, S. E.; Bell, R. R.; Alexander, R. W., Jr.; Ward, C. A. *Appl. Opt.* **1983**, *22*, 1099.

(3) Spitzer, W. G.; Kleinman, D. A. *Phys. Rev.* **1961**, *121*, 1324.

(4) Maeda, S.; Schatz, P. N. *J. Chem. Phys.* **1961**, *35*, 1617.

(5) Schatz, P. N. *J. Chem. Phys.* **1960**, *32*, 894.

0022-3654/86/2090-4499$01.50/0